J. Non-crystalline Solids, 358(4):728–734, 2012.

Sol-Gel Simulation–II: Mechanical Response

E. J. Barbero[1] and F. A. Campo[2]
Mechanical and Aerospace Engineering, West Virginia University,
Morgantown, WV 26506-6106, USA

Abstract

A novel computational procedure is proposed to predict the outstanding mechanical properties of sol-gel structures. An aggregation algorithm incorporating Brownian motion and chemical reactions is used to recreate the sol-gel structures at molecular scale. Just like in the physical colloidal aggregation process, the computational aggregation process produces structures with fractal features. Such fractal character leads to a recursion algorithm for calculating mechanical properties at any scale using a recursive multi scale approach. The mechanical properties are then predicted at each scale by calculating the effective properties using the finite element method. It is shown that Young modulus naturally follows a power law relationship with density, whereas Poisson's ratio displays more complicated behavior. Also, it is shown that Young modulus and Poisson's ratio depend on a) the mass distribution of the structure, which is influenced by the Brownian motion and chemical reactivity during the aggregation process, and b) the connectivity, which is also influenced by additional processes as sintering and/or aging. Finally, it is shown that the Young modulus and Poisson ratio can be correlated to scattering intensity of sintered and/or aged structures.

Keywords

Aerogel; Multi Scale; Fractal; Finite Element; Homogeneization

1 Introduction

Sol-gel technology, using colloidal aggregation, provides an efficient, green-manufacturing path for the fabrication of ceramic products [1, 2, 3, 4, 5, 6, 7, 8, 9, 10, 11, 12, 13]. Dense films, Aerogels, supercapacitors, and dense ceramics, to name some, are manufactured with this technology [14, 15, 16, 17, 18, 19, 20, 21, 22]. After extracting the liquid phase from the colloid, a solid ceramic structure remains. The resulting solid structure presents unique physical properties that are exploited for the fabrication of advanced products.

Gel-derived materials have been tested and characterized mechanically. Aerogel and xerogel experimental data for the Young modulus E as a function of the effective density ρ is available in [23, 24, 25, 26]. The experimental data fits well the power law equation (1), with b_E the scaling exponent of the Young modulus.

[1]Corresponding author. The final publication is available at http://dx.doi.org/10.1016/j.jnoncrysol.2011.12.005

[2]Graduate Research Assistant

$$\frac{E}{E_0} = \left(\frac{\rho}{\rho_0}\right)^{b_E} \tag{1}$$

Experimentally and computationally b_E is found in the range 2–4 [25, 26, 8] for aerogels and xerogels. However, these values appear to be high compared to the values predicted by classical models. Whereas for a dense material the Young modulus is independent of density, i.e. $b_E = 0$, it is shown in [26] that a Kevin-Voigt model predicts $b_E = 1$, i.e., a simple rule of mixtures relationship. The elastic behavior of low density sol-gel structure is explained in [26] through bending of the rods forming the structure as being the primary loading mechanism, resulting in a scaling factor $b_E = 2$. Theoretically, $b_E = 2$ is the highest value achievable in a fully connected structure, but this value turns out to be lower than the experimentally observed values.

Higher values of b_E were found theoretically in [26] and [25] by assuming that part of the mass contributing to the effective density does not plays a role in the elastic behavior, as it is the case of broken ends. Also, considering the elements composing the structure of the material as not necessarily straight rods, but rather curled twisted chains, implies an additional effect on b_E. Thus, [25] concludes that b_E satisfies (2).

$$b_E = \frac{5 - \mathcal{D}}{3 - \mathcal{D}} \tag{2}$$

where $\mathcal{D}$ is the fractal dimension characterizing an aggregated structure that takes into account bending of the elements, broken ends, and curled twisted chains. Although a fractal dimension must be in the range $(0 < \mathcal{D} < 3)$, for aerogels and xerogels, D is found typically in the range 1.8–2.4 depending on the pH during the aggregation process. However, experimentally measurements of $\mathcal{D}$ and E [24], reveal that not all experimental conditions satisfy (2).

In this paper a general calculation of the elastic behavior of sol-gel structures is presented. It is proposed that different responses (density, scattering, mechanical response) of gel-derived materials depend on different characteristics of the connected structure. The connected structure is understood as the collection of masses and bonds between them that form a network of particles. Each particle is identified by the functionality which is the number of particles that are next to it, and the coordination number which is the number of bonds that this particle has. Note that not all particles next to a particle need to be bonded. Thus, for the connected structure there is a functionality distribution and a coordination distribution. In [27], the coordination and functionality distributions were studied for different processing conditions. The processing conditions consist on the chemical part and the density. The chemical part of the processing conditions is contained in the reactivity, a number that measures how easy a particle with certain number of bonds forms a new bond when it collides to another particle, also with a certain number of bonds. The density is measured by the number of particles in a fixed volume determined for the simulation. In Part I [28], it was found that the fractal dimension $\mathcal{D}$ corresponds to a measure of the structure's mass distribution, however it is independent of structure's connectivity. In this paper, the stress-strain behavior is shown to depend also on the connectivity of the structure. For this purpose, density and mechanical response of computer generated structures that resemble gels and Aerogels are studied considering the different processing conditions rather than the fractal dimension only.

2 Computational Approach

2.1 Computer generated structures

The aggregation algorithm used to generate structures that resemble Aerogels[3] is explained in detail in [27]. Structures are generated inside a simulation box of size $L = 2a_0\lambda_{max}$, where $2a_0$ is the size of the primary particles, and λ_{max} the maximum scale analyzed. The scale λ is in the range $\lambda \in [1, \lambda_{max}]$.

The structure is generated by the aggregation of particles initially located randomly in a cubic lattice inside a simulation box. Periodic boundary conditions (PBC) are used to treat the simulation box as a representative volume element (RVE, [29, §4.1.2]). Particles are randomly chosen to move in the lattice, thus simulating Brownian motion. The coordination number and reactivity of the colliding particles (or clusters of particles) controls whether or not colliding particles/clusters bond or not, satisfying the Einstein-Smoluchowsky conditions [30, 31]. The value of the reactivity can be calculated from the change of energy required to form a bond. For high reactivities, reactions between clusters having many bonds are favored, whereas for low reactivity, reactions between clusters with few bonds are favored. Thus, the generated structure is more compact for higher reactivities, and more linear for low reactivities, as shown in [27] and confirmed by scattering experiments in [28].

2.2 Elastic Behavior

The elastic behavior of a structure is measured subjecting it to a set of uniform strain tests. A uniform displacements field is defined as [32]

$$u_i = \varepsilon^0_{ij}(x_j - x_{j0}) \tag{3}$$

where x_j is the position vector of any point, e.g. the position of a particle, and x_{j0} is a reference point where the displacement is zero. Then, uniform strains are defined as

$$\varepsilon_{ij} = \frac{1}{2}\left(u_{i,j} + u_{j,i}\right) = \varepsilon^0_{ij} \tag{4}$$

where $u_{i,j} = \partial u_i/\partial x_j$. Using contracted notation [33, (1.9)] as

$$\alpha = \begin{cases} i & \text{for } i = j \\ 9 - (i + j) & \text{for } i \neq j \end{cases} \tag{5}$$

yields the strain tensor $\varepsilon_\alpha = \varepsilon_{ij}$, the stress tensor $\sigma_\alpha = \sigma_{ij}$, and the stiffness tensor $C_{\alpha\beta} = C_{ijkl}$. The total energy $U(\varepsilon)$ stored in the system is measured simulating the structure using the Finite Element Method [34]. A typical structure generated using the aggregation algorithm is shown in Figure 1(a) and its geometrical representation using the finite element method is shown in Figure 1(b).

For small strains, the total energy stored in the system can be expanded with a Taylor series[4][33] as follows,

$$\frac{1}{V}U(\varepsilon) \approx \varepsilon_\alpha \left(\frac{1}{2}C'_{\alpha\beta}\right)\varepsilon_\beta \tag{6}$$

[3] Modeling Xerogels and thin films requires modifying the algorithm in [27] by including the removal of the liquid phase, taking into account that, as opposed to the case of Aerogel, the liquid removal from a Xerogel is not as gentle.

[4] The first order derivatives vanish at the equilibrium state because the exerted force at that point is zero.

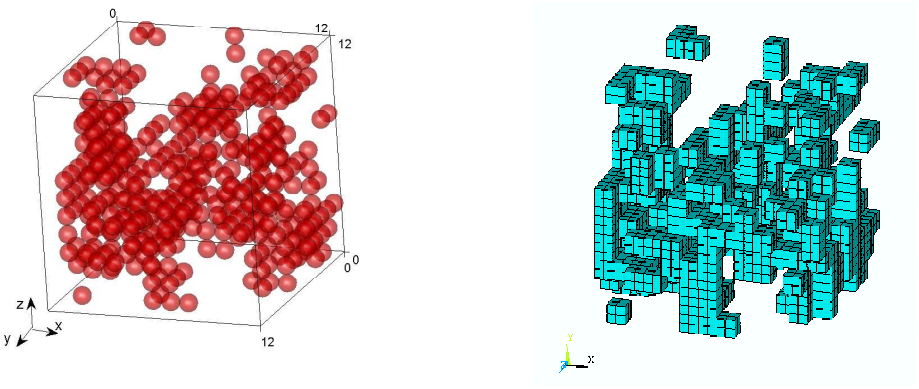

(a) Structure from aggregation algorithm (b) Finite Element Model

Figure 1: Structure generated with $N = 400$ particles and reactivity $w = 1.0$.

where V is the volume of the simulation box. Note that each of the components of stiffness tensor C_{lm} can be extracted using its symmetry

$$C_{lm} = \frac{1}{2}\left(C'_{lm} + C'_{ml}\right) = C_{ml} \tag{7}$$

and using the fact that the stiffness can be derived from the potential function U as

$$C_{lm} = \frac{1}{V}\frac{\partial^2 U}{\partial\varepsilon_l\,\partial\varepsilon_m} \tag{8}$$

To measure the 21 stiffness constants of the anisotropic structure, 21 tests combining all the possible $u^k_{i,j}$ are performed, thus recreating all the possible pairs $\varepsilon_\alpha\varepsilon_\beta$. From the set of energies U^k obtained, the solution of the system

$$\frac{1}{V}U^k = \varepsilon^k_\alpha C_{\alpha\beta}\varepsilon^k_\beta \tag{9}$$

gives the values of $C_{\alpha\beta}$.

Assuming that the material is composed of a random aggregation of structures like the ones produced with the algorithm described in Section 2.1, when subjected to a load, the strain-energy is absorbed in average by each of the composing structures proportionally to their volume. In other words, the energy density can be assumed spreads homogeneously, satisfying the equipartition energy theorem [35, 36] and the Boltzmann postulate[5][37, 38]. Hence, the total energy is the summation of the energy of the parts as

$$\begin{aligned} U_{tot}(\varepsilon) &= \sum U(\varepsilon) \\ V_{tot}\,\mathcal{H}\left(C_{\alpha\beta}\right)\varepsilon_\alpha\varepsilon_\beta &= \sum V^{(e)} C^{(e)}_{\alpha\beta}\varepsilon_\alpha\varepsilon_\beta \end{aligned} \tag{10}$$

Therefore, for $V_{tot} = \sum V^{(e)}$, for structures with the same volume, and for N_s samples, $N_s = V_{tot}/V^{(e)}$, the total effective stiffness matrix can be calculated as

[5]The Boltzmann postulate states that microstates with equal energy have the same probability of occurrence.

$$\mathcal{H}\left(C_{\alpha\beta}\right) = \frac{1}{N_s}\sum_{e}^{N_s} C_{\alpha\beta}^{(e)} \tag{11}$$

where $\mathcal{H}\left(\right)$ represents the proposed process of homogenization and averaging.

According to the argument posed in [28, §4], the fractal character makes sense only for the critical percolation concentration, meaning that the mechanical response needs to be calculated at this concentration. As discussed in [28, §4], the aggregation process can be classified into three regimes depending on the number of particles N inside the simulation box and the fractal dimension $\mathcal{D}$: i) if there are less particles than a critical percolation density [28, eqs. 5 and 12], the final aggregate results in isolated clusters suspended inside the simulation box, ii) if there are just enough particles, the aggregate percolates, i.e., it spans the simulation box and connects the faces of the box, and iii) if there are more particles than the critical percolation density, the simulation produces more compact structures, with fractal dimension higher than what is should be–that is, without the limitations of the simulation box, the physical colloid would aggregate a larger cluster with critical percolation density. Thus, because of the constraint imposed by the simulation box, only at the critical percolation density the structure can aggregate with a fractal dimension congruent with the chemistry of the aggregation process. Since the simulation box has fixed dimensions, an interpolation allows us to find the mechanical response at the critical percolation density.

Using the fractal character of the structure, the effective density is

$$\rho = \rho_0 \left(\frac{\xi}{2a_0}\right)^{D-3} \tag{12}$$

where ξ is the correlation length determined by the aggregation parameters [28, §3–4], and ρ_0 is the density of the primary particle. Note, that the correlation length of the clusters can be written as

$$\frac{\xi}{2a_0} = \left(\frac{L}{2a_0}\right)^{n} \tag{13}$$

where n is the number[6] of times (generations) that the structure is composed of itself. Hence,

$$n = \frac{\log \frac{\xi}{2a_0}}{\log \frac{L}{2a_0}} \tag{14}$$

Therefore, (12) is rewritten as

$$\frac{\rho}{\rho_0} = n_0^{\frac{\log \frac{\xi}{2a_0}}{\log \frac{L}{2a_0}}} \tag{15}$$

In a more general scheme, assuming that n is an integer, at each generation (i), (15) can be calculated from the recurrence

$$\rho^{(i+1)} = \rho^{(i)} n_0(w) \tag{16}$$

with $\rho^{(0)} = \rho_0$.

[6] Formally, n is not necessarily an integer.

N	100	200	400	800	1600	1728	
w	0.1	0.2	0.4	0.8	1	1.2	1.6
λ_{max}	12						

Table 1: Parametric test conditions: N is the number of particles in the simulation box of of size $L = 2\,a_0\lambda_{max}$, and w is the reactivity.

Using the procedure explained in Section 2.2, the stiffness can be calculated sequentially at each generation by introducing the effective stiffness calculated during the previous generation as the stiffness of the primary cluster for the current generation. This means that the effective stiffness can be calculated from the proposed homogenization $\mathcal{H}$ and recurrence as

$$C_{\alpha\beta}^{(i+1)} = \mathcal{H}\left(C_{\alpha\beta}^{(i)}\right) \tag{17}$$

with $C_{\alpha\beta}^{(0)} = C_{\alpha\beta 0}$. In this way, the relationship between the mechanical response and density can be calculated for a correlation length several orders of magnitude larger than the simulation box, i.e. $\xi >> L$.

3 Computational Results: Elastic Behavior

Silica Aerogels are simulated for the conditions in Table 1 using amorphous silica as primary particle at molecular level. An example of the resulting structure is presented in Figure 1(a). For Aerogels in this work, Young modulus $E = 80\,GPa$ and Poisson's ratio $\nu = 0.22$ is used [39]. The simulation is performed using ANSYS [34] for two cases: 1) *as-gelled structures* and 2) *fully connected structures*. In as-gelled structures, the bonds are the result of the aggregation process; not all of the potential bonds between colliding particles are formed. In fully connected structures, the missing bonds of the as-gelled structure are allowed to materialize, either by ageing or sintering.

Von Misses stress contour plots are shown in Figure 2 for both types of structures subjected to $\epsilon_{xy} = 1$. Note that the as-gelled structure has missing bonds that prevent the structure from effectively transferring stress, while the fully connected structure displays a more uniform state of stress as a result of the ability of the structure to transfers stress along all possible paths.

After averaging 32 specimens for each sample of the 42 conditions listed in Table 1, the effective mechanical behavior was found to be isotropic.

For reactivity $w = 1$, effective Young modulus and effective Poisson ratio[7] as a function of the number of particles are presented in Figures 3 and 4, respectively. As-gelled structures are produced by the aggregation algorithm described in [27]. Fully connected structures are then obtained by simulated sintering and/or aging[8].

Mechanical properties are shown in Figures 3 and 4 for different generations. Note that the fully connected structures present a higher Young modulus and Poisson's ratio compared to the structure as gelled for the same conditions. Also, in fully connected structures, both Young modulus and Poisson's ratio decrease with decreasing number of particles. However, in as-gelled structures, only the Young modulus decreases with decreasing number of particles.

With each generation, the Young modulus reduces a constant amount in logarithmic scale (Figure 3). This suggests that the Young modulus follows a power law as a function of generations.

[7] $E = 1/S_{11}$ and $\nu = -S_{12}/S_{11}$, where $S = C^{-1}$ is the compliance tensor.

[8] Sintering and aging are simulated by adding the missing bonds between neighboring particles.

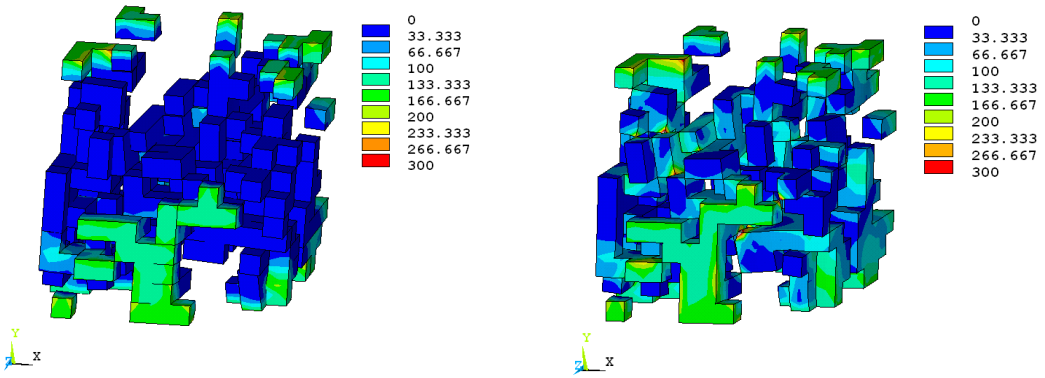

(a) As Gelled (b) Fully Connected

Figure 2: Von Misses plot for structure as gelled and fully connected structure for $w = 1.0$ and $N = 400$.

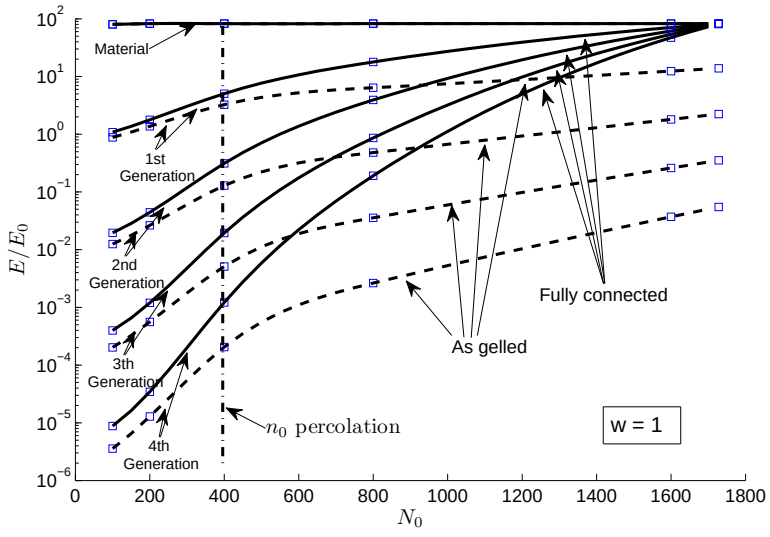

Figure 3: Effective Young modulus for the structures as a function of the number of particles. Lines are splines used as guide to the eyes.

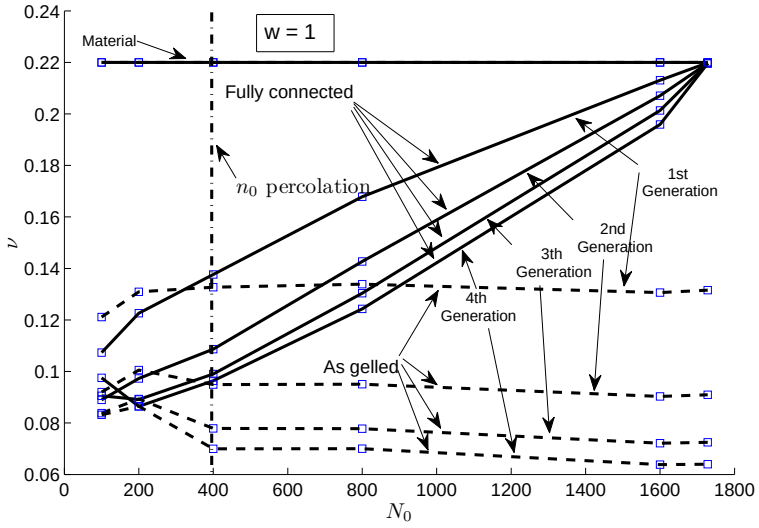

Figure 4: Effective Poisson ratio for the structures as a function of the number of particles. Lines are used as guide to the eyes.

This is not the case for the Poisson's ratio. In addition, note that for fully connected structures, as the number of particles reaches the limit in the simulation box, i.e. 1728 particles for $L = 12$, the properties approach the properties of the constituent material. On the contrary, for the structures as gelled, this trend is not observed because there are missing bonds. Aging/sintering lets the structure form all its bonds and the properties of the primary particle are recovered when the simulation box is fully dense.

The effect of aging/sintering is seen over the entire range of N in Figure 3. As $N \to 0$, the stiffness should approach zero. For very low values of N, the splines used to fit the data in Figure 3 do not capture such trend exactly, but the computational evaluation of the stiffness does captures this effect as the homogenization over an empty simulation box produces zero stiffness.

Density ρ vs. the generation number n are shown in Figure 5 for different reactivities. It can be seen that density reduces with each successive generation. This is because the effective density of a cluster is less than the density of the primary particle, and each successive generation uses the cluster of the previous generation as primary particle. Also, for higher reactivities, the effective density is higher as the fractal dimension is higher [27].

As the density reduces with generations, so do the mechanical properties, as shown in Figures 3 and 6. Of course this effect is more notable when the number of particles is small because then the effective density at each generation is much smaller than the density of the primary particle. Recursion just magnifies this effect, as it is clearly seen on the left of Figures 3 and 6.

Another observation can be made regarding percolation. In Figure 3, the vertical line indicates the critical number of particles in the simulation box for which the structure percolates, as revealed by scattering simulation in [27]. The structures to the left of the vertical line do not percolate, and show an accentuated decrease in the Young modulus for each generation when compared to the structures that percolate. The mechanical properties of the fully connected structures reduce faster than the as-gelled ones because un-percolated structures are disconnected, and thus inefficient to generate mechanical properties. Therefore, in this range, aged/sintered structures behave closer to as-gelled structures, the later having even more disconnected structure. On the contrary, to the

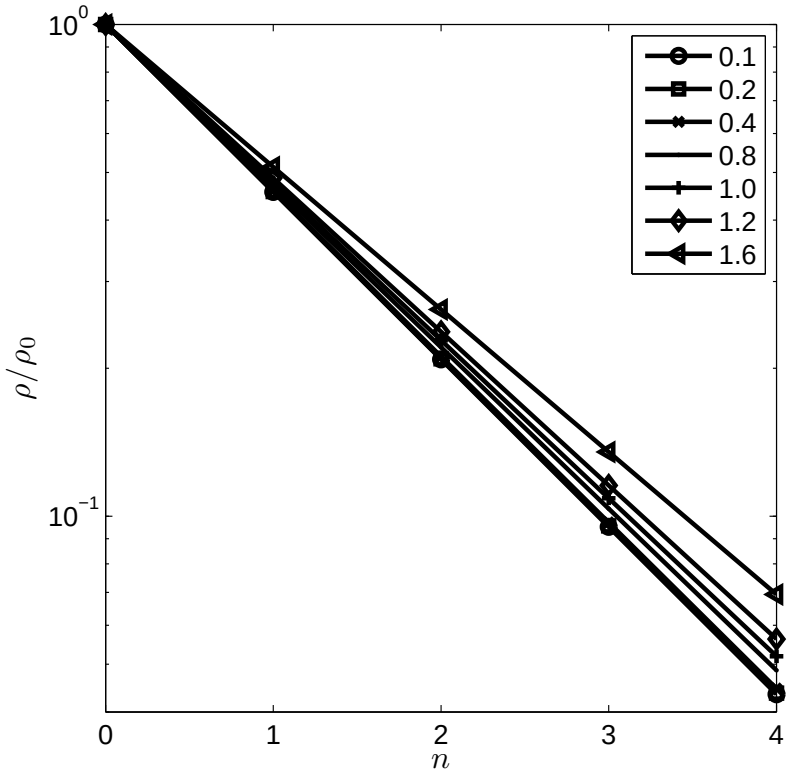

Figure 5: Density ρ vs. number of generations n for different reactivities. Lines are used as guide to the eyes.

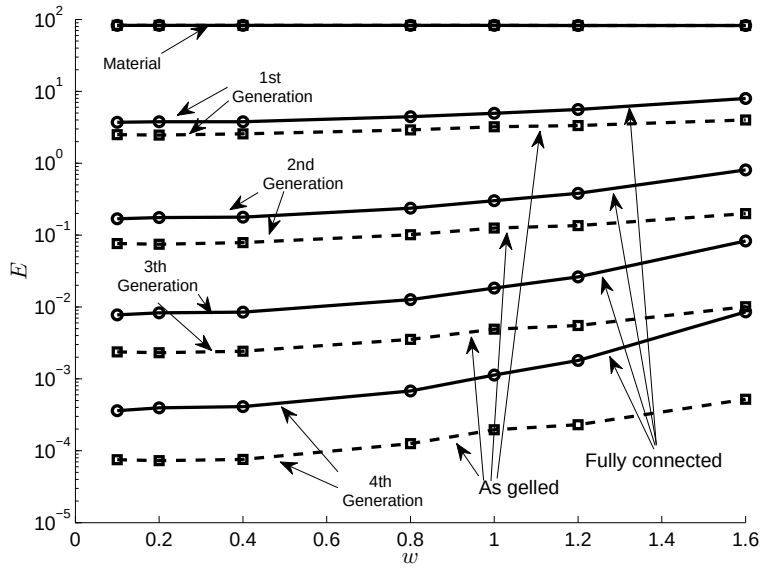

Figure 6: Effective Young modulus as a function of the reactivity, at critical percolation concentration. Lines are used as guide to the eyes.

right of the critical percolation density line, percolated aged/sintered structures are more efficient in carrying load, with higher mechanical properties, whereas as-gelled structures have some amount of disconnected structure.

In contrast to the Young modulus trend observed, Poisson's ratio is not affected appreciably by percolation, as shown in Figure 4, since the strain coupling between two directions is a local effect. Percolation, which is a global effect, measures the connectivity that the structure generates between faces of the simulation box.

Although not displayed in Figure 3 and 4, similar trends were observed for other values of reactivity.

Effective Young modulus and effective Poisson's ratio are shown in Figures 6 and 7 as a function of reactivity, at the critical percolation concentration. For all reactivities, there is a slight improvement of the Young modulus and Poisson's ratio as the reactivity increases. Note how the properties of the fully connected structure are higher than the properties of the as-gelled structure, for every generation.

In Figures 8 and 9, effective Young modulus and effective Poisson's ratio are presented as a function of effective density. The power law relationship between effective Young modulus and effective density is clearly seen in Figure 8. Young modulus and Poisson's ratio are clearly higher for fully connected structures than for as-gelled structures. Also, for fully connected structures, Young modulus and Poisson's ratio are higher as the reactivity increases at constant density, whereas the opposite is observed for as-gelled structures.

4 Discussion

Effective Young modulus of the as-gelled and fully connected structures as a function of effective density, shown in Figure 8, can be represented by the power law in (1). Values of the scaling exponent b_E as a function of reactivity are presented in Figure 10. Similarly to [8, 25], the scaling

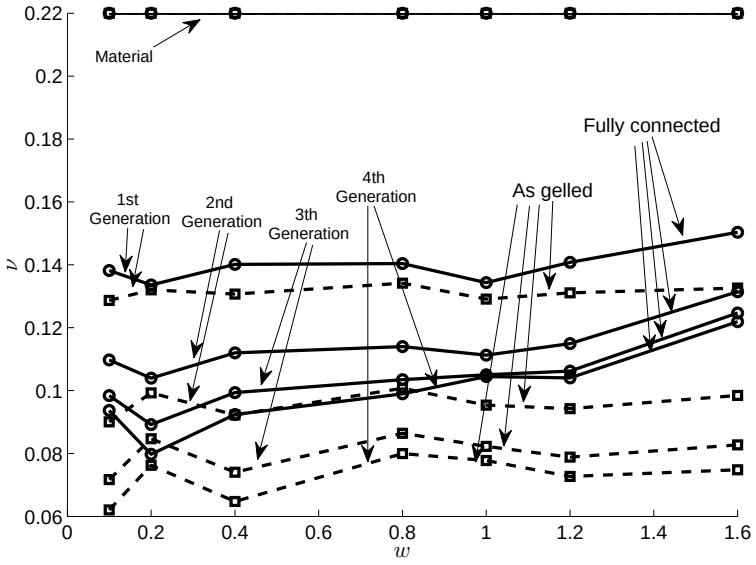

Figure 7: Effective Poisson ratio as a function of the reactivity for the critical percolation concentration. Lines are used as guide to the eyes.

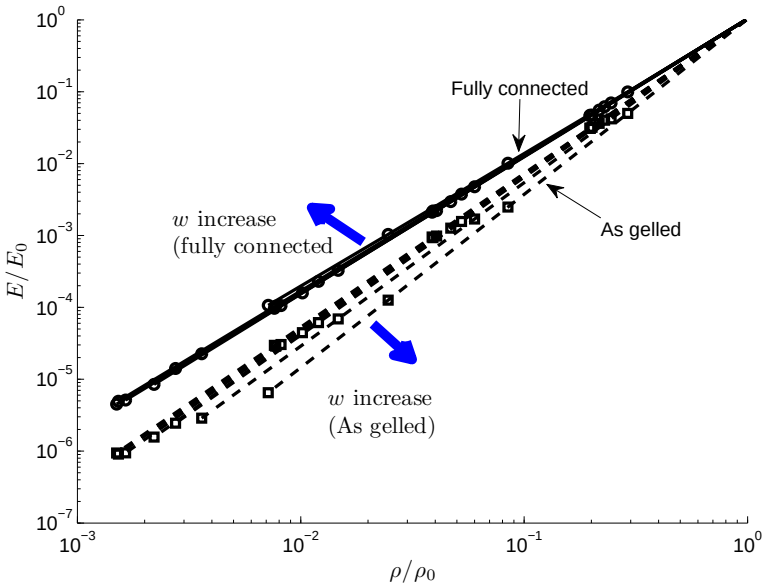

Figure 8: Effective Young modulus as a function of the effective density. Lines are used as guide to the eyes.

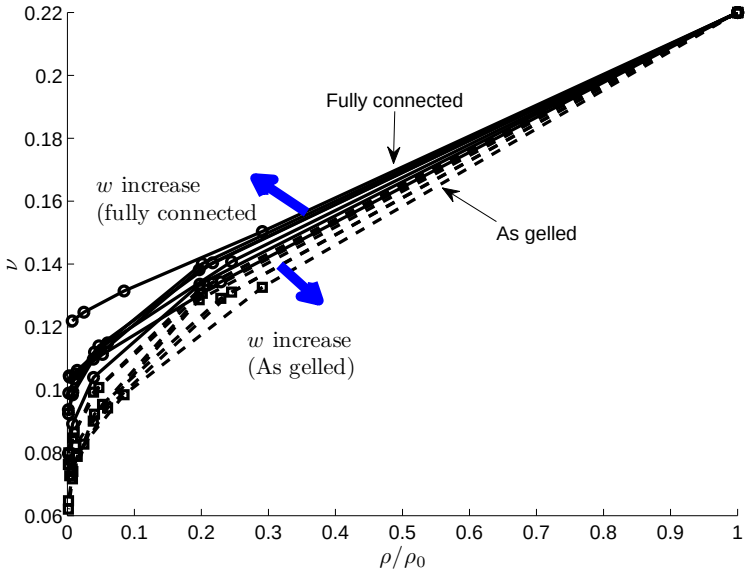

Figure 9: Effective Poisson ratio as a function of the effective density. Lines are used as guide to the eyes.

exponents are found in the range 2–4. It is clear that the connectivity of the structure plays a crucial role in the mechanical response for the same mass distribution. Fully connected structures have a smaller amount of mass that is not affected mechanically when the structure is loaded, compared to structures with cracks, as it is the case of as-gelled structures. As a matter of fact, if the relaxed mass of a loaded structure is removed, more mass would be removed from structures with cracks than from fully connected structures. Thus, the effective fractal dimension of the remaining structure must be smaller than the fractal dimension measured from scattering experiments that considers the whole mass distribution. Hence, the numerator of (2) requires a reduced value of the fractal dimension $\mathcal{D}_E < \mathcal{D}$ that is not measured from scattering experiments, whereas the denominator, deduced form the scaling of the density, remains identical. For the fully connected structure, $\mathcal{D}_E = \mathcal{D}$. Therefore, (2) may be rewritten as

$$b_E = \frac{5 - \mathcal{D}_E}{3 - \mathcal{D}} \tag{18}$$

where $\mathcal{D}_E$ is a measure of the connectivity of the structure.

In Part I [27] it was shown that the fractal dimension of the structures increases with the reactivity. Since, for the range of reactivities studied, the fractal dimension does not changes very much, the loading mechanism of the elements (bending, shear, compression) remain the same. Figure 10 allows us to correlate the processing conditions and the structure at these conditions. The invariance of b_E for fully connected structures means that the reactivity (which contains the chemical information of the aggregation process) does not makes the structure behave more or less elastically efficiently as it gets denser. In contrast, the as-gelled structure is weakened by the addition of intrinsic cracks as it gets denser. The weakening effects are more important as the reactivity increases because the structure is more compact for higher reactivities, i.e. at higher fractal dimensions.

In principle, a direct correlation between mechanical response and scattering intensity seems

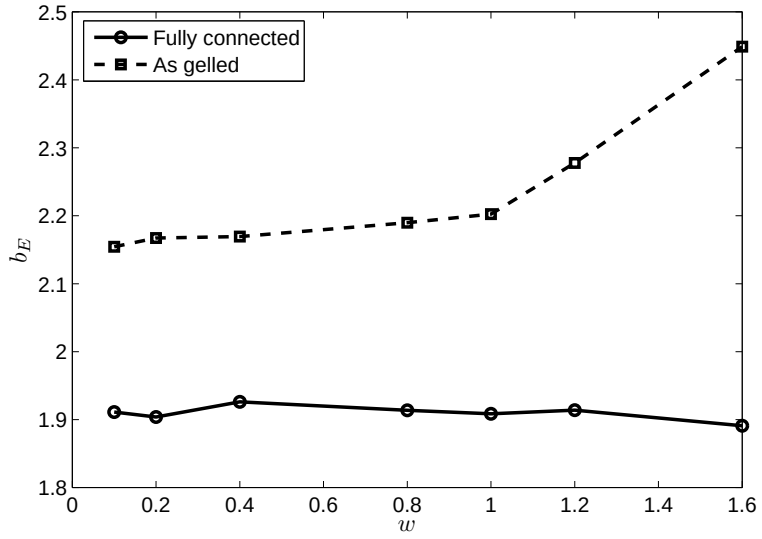

Figure 10: Power law exponent as a function of reactivity. Lines are used as guide to the eyes.

not to exist. The mechanical response depends directly on the connectivity of the structure whereas scattering intensity depends directly on mass distribution. However, knowing that for fully connected structures the connectivity is given by the mass distribution [27], the mechanical properties are seen to depend uniquely on mass distribution. Thus, scattering intensity and mechanical behavior of fully connected structures are directly correlated. For aged/sintered structures, all what is needed to predict the mechanical response is available in the scattering response.

Future work may entail using the percentage of missing bonds between colliding particles to correlate the coordination to the functionality distribution. In doing so, one would be able to predict the mechanical behavior of as-gelled structures using their scattering response. So far, the use of scattering experiments allows us to partially predict the mechanical response of sol-gel structures by measuring their correlation length and fractal dimension. However, it is emphasized that mechanical behavior cannot be fully derived from scattering experiments unless connectivity and mass distribution are correlated. The exception to this observation are sintered and/or aged structures where the coordination distribution and the functionality distribution coincide.

5 Conclusions

The mechanical properties of the sol-gel vary, depending on the aggregation process, as a function of reactivity and amount of precursor, thus determining the connectivity and correlation length of the structure. Additional processes such as sintering and/or aging modify the connectivity of the structure maintaining the same mass distribution of the structure. In this way, sintering and/or aging strengthens the structure by forming the missing bonds between particles that are next to each other. In this work, the two limiting cases where studied: the as-gelled structure with the lowest mechanical properties, and the fully connected structure with the highest mechanical properties. Aging or sintering produces a structure where scattering intensity and mechanical response are fully correlated to each other. When, due to ageing or sintering, the missing bonds of the as-gelled structure become active bonds, the whole mass of the structure (as seen by scattering) contributes to the mechanical behavior of the material.

Both scattering intensity and mechanical response reveal a fractal character for both as-gelled and fully connected structures. Thus, the calculation of the mechanical response for a large structure with a large amount of features can be performed using a recursive procedure. The recursive procedure shows that the stiffness components follow a more complex relationship than a power law. Such complex behavior is explained by the coupling between the stiffness components through Poisson's effects. Finally, producing a mechanically efficient structure is a compromise between the mechanical improvement due to structure's mass distribution (lower fractal dimension behaves better), improved connectivity (less cracks), and higher density.

References

References

[1] R. Orbach, Dynamical properties of fractal networks: Scaling, numerical simulations, and physical realizations, Rev. Mod. Phys. 66 (2) (1994) 381–443.

[2] V. Zosimov, L. Lyamshev, Fractals in wave processes, Physics - Uspekhi 38 (4) (1995) 347–384.

[3] E. Vinogradova, A. Moreno, H. Lara, P. Bosch, Multi-fractal imaging and structural investigation of silica hydrogels and aerogels, Silicon Chemistry 2 (2003) 247–254.

[4] A. E. Gonzalez, G. Ramirez-Santiago, Scaling of the structure factor in fractal aggregation of colloids: Computer simulations, Journal of Colloid and Interface Science 182 (1996) 254–267.

[5] R. Jullien, M. Kolb, Hierarchical model for chemically limited cluster-cluster aggregation, J. Phys. A: Math Gen. 17 (1984) L639–L643.

[6] R. Botet, R. Jullien, M. Kolb, Hierarchical model for irreversible kinetic cluster formation, J. Phys. A: Math Gen. 17 (1984) L75–L79.

[7] M. Kallala, R. Jullien, B. Cabane, Crossover from gelation to precipitation, Phys II France 2 (1992) 7–25.

[8] J. Rivas-Murillo, M. Bachlechner, F. Campo, E. Barbero, Structure and mechanical properties of silica aerogels and xerogels modeled by molecular dynamics simulation, J. Non-Cryst. Solids 356 (2010) 1325–1331.

[9] M. Bruno, N. Cotella, M. Miras, T. Koch, S. Seidler, C. Barbero, Characterization of monolithic porous carbon prepared from resorcinol/formaldehyde gels with cationic surfactant, Colloids and Surfaces A: Physicochemical and Engineering Aspects 358 (1-3) (2010) 13 – 20. doi:DOI:10.1016/j.colsurfa.2010.01.017.

[10] J. T. Seo, Q. Yang, S. Creekmore, B. Tabibi, D. Temple, S. Y. Kim, K. Yoo, A. Mott, M. Namkung, S. S. Jung, Large pure refractive nonlinearity of nanostructure silica aerogel, Applied Physics Letters 82 (2003) 4444–4446. doi:10.1063/1.1585127.

[11] X. Li, S. E. Rankin, Multiscale dynamic monte carlo/continuum model of drying and nonideal polycondensation in sol-gel silica films, AIChE J. 56 (11) (2010) 2946–2956.

[12] S. Corezzi, D. Fioretto, C. De Michele, E. Zaccarelli, F. Sciortino, Modeling the crossover between chemically and diffusion-controlled irreversible aggregation in a small-functionality gel-forming system, The Journal of Physical Chemistry B 114 (11) (2010) 3769–3775.

[13] D. Fry, A. Mohammad, A. Chakrabarti, C. M. Sorensen, Cluster shape anisotropy in irreversibly aggregating particulate systems, Langmuir 20 (18) (2004) 7871–7879.

[14] C. Brinker, G. Scherer, Sol-Gel Science. The Physics and chemestry of Sol-Gel Processing, Academic Press, New York, USA, 1990.

[15] L. W. Hrubesh, Aerogel applications, J.Non-Cryst. Solids 225 (1998) 335–342.

[16] J. Fricke, A. Emmerling, Aerogels – recent progress in production techniques and novel applications, J. Sol-Gel Sci. Technol. 13 (1998) 299–303.

[17] R. P. Patel, N. S. Purohit, A. M. Suthar, An overview of silica aerogels., International Journal of ChemTech Research 1 (4) (2009) 1052 – 1057.

[18] A. Martucci, D. Buso, M. Monte, M. Guglielmi, C. Cantalini, C. Sada, Nanostructured sol-gel silica thin films doped with NiO and SnO2 for gas sensing applications, Journal of Materials Chemistry 14 (2004) 2889–2895.

[19] Y. K. Akimov, Fields of application of aerogels (review), Instrum. Exper. Techniques 46 (2003) 287.

[20] G. Dominguez, A. Westphal, M. L. F. Phillips, S. Jones, A fluorescent aerogel for capture and identification of interplanetary and interstellar dust, Astrophys. J 592 (2003) 631–635.

[21] D. Pope, NASA puts the heat on aerogels, Ind. Physicist 3 (1997) 13.

[22] C. Sanchez, C. Boissire, D. Grosso, C. Laberty, L. Nicole, Design, synthesis, and properties of inorganic and hybrid thin films having periodically organized nanoporosity, Chemistry of Materials 20 (3) (2008) 682–737.

[23] T. Woignier, F. Despetis, Mechanical properties of gel-derived materials, J. Sol-Gel Sci. Technol. 19 (2000) 163–169.

[24] T. Woignier, J. Reynes, A. H. Alaoui, I. Beurroies, J. Phalippou, Different kinds of structure in aerogels: relationships with the mechanical properties., Journal of Non-crystalline Solids 241 (1998) 45–52.

[25] A. Emmerling, J. Fricke, Scaling properties and structure of aerogels, Journal of Sol-Gel Science and Technology 8 (1997) 781–788.

[26] J. Gross, J. Fricke, Scaling of elastic properties in highly porous nanostructured aerogels, NanoStructured Materials 6 (1995) 905–908.

[27] F. Campo, J. R. Murillo, E.J.Barbero, Aggregation model for the gelation of a sol starting from the processing conditions, Journal of Non-crystalline Solids 357 (2011) 2046–2053. doi:10.1016/j.jnoncrysol.2011.02.025.

[28] F. A. Campo, E. J. Barbero, Sol gel simulation–I: Scattering response, Journal of Non-crystalline Solids.doi:http://dx.doi.org/10.1016/j.jnoncrysol.2011.10.023.

[29] E. J. Barbero, Introduction to Composite Materials Design, 2nd Edition, CRC Press. Taylor & Francis Group, USA, 2010.

[30] R. Mazo, Brownian Motion. Fluctuations, Dynamics and Applications., Oxford University Press, New York, USA, 2002.

[31] F. Spitzer, Principles of Random Walk, 2nd Edition, Springer-Verlag, New York, USA, 2001.

[32] J. Aboudi, Mechanics of Composite Materials. A Unified Micromechanical Approach. Studies in Applied Mechanics. Vol 29, Elsevier, The Netherlands, 1991.

[33] E. J. Barbero, Finite Element Analysis of Composite Materials, CRC Press. Taylor & Francis Group, USA, 2008.

[34] ANSYS, Academic research. release 12.0.

[35] D. P. Landau, K. Binder, A Guide to Monte Carlo Simulations in Statistical Physics, Cambridge University Press, United Kingdom, 2000.

[36] H. B. Callen, Thermodynamics and an Introduction to Thermostatics, 2nd Edition, John Wiley Sons, New York, USA, 1985.

[37] L. Reichl, A Modern Course in Statistical Physics, 2nd Edition, Wiley-VCH Verlag GmbH & Co. KGA, Weinheim. Germany, 2004.

[38] J. Hansen, I. McDonald, Theory of Simple Liquids, 6th Edition, Academic Press, Great Britain, 1986.

[39] L. Freund, S. Suresh, Thin film materials, Cambridge University Press, 2003.